The ice content of the Dorsa Argentea Formation from radar sounder data

Jennifer L. Whitten[1], Bruce A. Campbell[2], Jeffrey J. Plaut[3]

[1]Department of Earth and Environmental Sciences, Tulane University, New Orleans, LA 70118
ORCID: 0000-0001-8068-9597
[2]Center for Earth and Planetary Studies, National Air and Space Museum, Smithsonian Institution, Washington, D. C. 20560
[3]NASA Jet Propulsion Laboratory, California Institute of Technology, Pasadena, CA 91109

Key Points:

- Loss tangent values are consistent with the DAF being largely composed of volatile-poor material.
- MARSIS reflections provide evidence that the DAF continues underneath the SPLD.
- Most water ice deposits have not persisted in the DAF through large changes in obliquity.

Resubmitted to
Geophysical Research Letters
November 6, 2020

1. Abstract

The Dorsa Argentea Formation (DAF) is an extensive Hesperian plains unit in the south polar region of Mars that was once ice-rich and may still contain a substantial fraction of water ice. Given its 3.5-Ga age, the possibility for massive ice in the DAF has significant implications for the preservation of volatiles during large obliquity changes. Here MARSIS and SHARAD radar sounder data are analyzed to determine whether massive water ice is present at depth by utilizing subsurface DAF reflectors to infer the loss tangent of overlying material. SHARAD (0.005±003) and especially MARSIS (0.009±006) loss tangent values are closer to those of dry sediment than to equatorial glaciers or the polar caps, but a fraction of remnant ice at depth may occur. Water ice is not the predominant component of the DAF, so much of the ancient ice has been lost during large obliquity changes over the past 3.5 Ga.

Plain Language Summary

The Dorsa Argentea Formation (DAF) is a 3.5 billion-year-old plains deposit that surrounds the south polar ice cap on Mars. The DAF was once ice-rich and may still contain a large fraction of water ice below the surface. The possibility that ancient ice is preserved in the subsurface of the DAF has implications for the climate history of Mars, especially how warm the polar regions were in the past. Here we analyze MARSIS and SHARAD radar sounder data to determine whether water ice is present. Radar sounder data provides detailed information about materials beneath a planetary surface. The MARSIS and SHARAD data reveal a greater similarity of the DAF to dry sediments than to pure water ice. Much of the ancient ice has been lost over the history of the DAF due to changes in the polar tilt of Mars.

2. Introduction

The south polar region of Mars likely contains one of the longest climate records on Mars. The polar geologic record is bookended by the Amazonian CO_2 ice deposits superposed on the south polar layered deposits (SPLD) and the Hesperian-aged Dorsa Argentea Formation (DAF). The DAF presents possibly the best record of ancient climate in the polar regions of Mars, being the oldest plains unit at either pole. While the ~3.5 Ga DAF (Plaut et al., 1988; Kress and Head, 2010) has been proposed to have formed by a variety of processes, including volcanism (Tanaka and Scott, 1987), debris flows (Jöns, 1992; Tanaka and Kolb, 2001), aeolian deposition (Tanaka and Scott 1987), and glacial activity (Kargel and Strom, 1992; Head and Pratt, 2001; Milkovich et al., 2002; Ghatan and Head, 2004; Scanlon et al., 2018), most recent research has converged on a glacial origin for the DAF. Formation by glacial processes strengthens the argument that the DAF may preserve a signature of past climates in an ancient ice record.

The DAF (Fig. 1) is a circum-SPLD plains deposit (Tanaka and Scott, 1987) with a variety of superposed landforms that support the glacial formation hypothesis. Perhaps the most notable are the Dorsa Argentea (Tanaka and Kolb, 2001), the namesake of the deposit, which are ridges generally interpreted as eskers (Howard, 1981; Butcher et al., 2016). Eskers are sediment ridges that form when meltwater flows underneath ice sheets and glaciers. Other superposed landforms on the DAF include pedestal craters (Bleacher et al., 2003; Kadish et al., 2011), subglacial edifices (Tanaka and Scott, 1987; Ghatan and Head, 2002) and heavily pitted terrain (Sisyphi Cavi, Cavi Angusti) (Dickson and Head, 2006), all of which indicate the escape of volatiles from the subsurface. Preliminary analyses of radar sounder data indicated the possibility of water ice within the DAF subsurface, suggesting a 3.5 billion-year-old mass of preserved ice (Plaut et al., 2007a). The current interpretation of the DAF as the remnants of an ancient ice sheet implies that there were multiple polar ice caps that existed at discrete periods of time in martian history, and that portions of these ancient deposits may have persisted in the subsurface through various changes in orbital parameters, such as obliquity (Laskar et al., 2004).

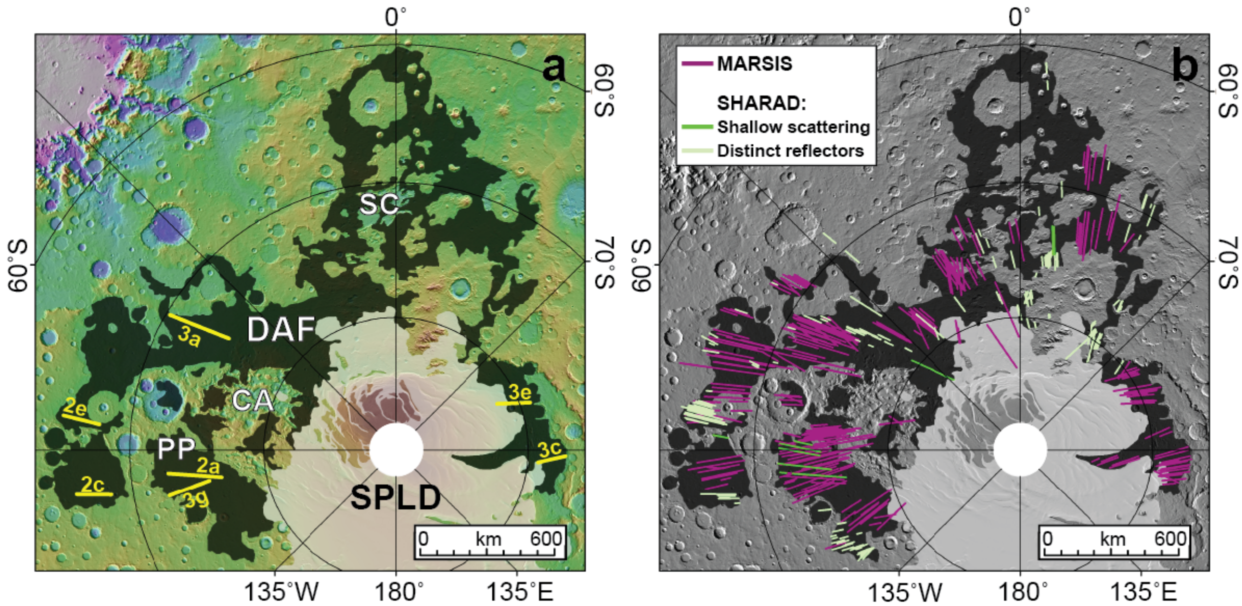

Figure 1. Areal distribution of the Dorsa Argentea Formation (black) in the south polar region of Mars (a) and detected subsurface reflectors from the MARSIS and SHARAD instruments (b). (a) SC = Sisyphi Cavi, CA = Cavi Angusti, PP = Parva Planum; MOLA 128 ppd hillshade overlain by topography. (b) The two shades of green SHARAD lines note the locations of the two reflector types identified (see Fig. 2). Geologic units from Tanaka and Scott (1987) and Skinner et al. (2006). The location of SHARAD and MARSIS segments in Figures 2 and 3 are noted in yellow.

3. Data and Methods

Since the preliminary radar sounder analyses of the DAF, more than a decade of data has been collected, increasing the density of coverage over the south polar region of Mars. These additional data facilitate the assessment of the abundance and areal extent of water ice in the subsurface. Here, we analyze both the Mars Advanced Radar for Subsurface and Ionosphere Sounding (MARSIS) and Shallow Radar (SHARAD) sounder data to broadly determine the composition of the DAF.

3.1. Radar datasets

Radar sounder data are used to measure the surface and subsurface radiophysical properties of planetary bodies. The frequency of a radar sounder instrument, along with the material properties of a planetary surface, determines the penetration depth of a microwave signal. SHARAD is a radar sounder instrument onboard the NASA Mars Reconnaissance Orbiter mission (Seu et al., 2004) with a central frequency of 20 MHz and a bandwidth of 10 MHz. The horizontal spatial resolution of SHARAD is higher than MARSIS, with an along-track resolution of 0.3–1.0 km after synthetic aperture processing and 3–6 km in the cross-track direction. The vertical resolution of SHARAD is ~15 m in free space and 8–10 m in geologic materials. The MARSIS instrument on ESA's Mars Express mission has four frequency bands centered at 1.8, 3, 4, and 5 MHz with a 1 MHz bandwidth (Picardi et al., 2004). These data have an along-track resolution of 5–10 km after onboard processing and a cross-track footprint of 10–30 km. MARSIS has a vertical resolution of ~150 m in free space, or ~50–105 in geologic materials. MARSIS radargrams were processed using techniques described in Campbell and Watters (2016), and data from Bands 3 and 4 (the 4 and 5 MHz bands, respectively) were used for this analysis.

MARSIS and SHARAD tracks over the south polar region of Mars were searched for subsurface reflections within the bounds of the DAF mapped by Tanaka et al. (2014). The extent, power, and depth of those reflectors were tabulated for use in the loss tangent and dielectric constant analyses. Possible subsurface reflectors are compared with clutter simulations that help to avoid mapping spurious off-nadir returns (Choudhary et al., 2016).

3.2. Dielectric Properties: Loss Tangent

The loss tangent across Mars is strongly influenced by the composition of a material or mixture, with ice having very low loss and basaltic lava flows much higher values (Campbell and Morgan, 2018). Loss tangent values are calculated for reflectors identified in the MARSIS dataset, as well as a subset of the SHARAD data with obviously dipping reflectors (Text S1). A depth-averaged loss tangent can be calculated for buried layers where the subsurface reflector occurs over a range of round-trip time delay and assuming the material in between the surface and subsurface reflectors is uniform. Loss tangent values were calculated using:

$$\tan\delta = \frac{-\lambda}{2\pi c}\ln\left(10^{L/10}\right) \qquad (2)$$

where L is the observed power loss, c is the speed of light in a vacuum, and λ is the free space radar wavelength (15 m for SHARAD and 150 m for MARSIS) (e.g. Campbell et al., 2008). The observed power loss, L, is the slope of the line from a plot of reflector power (in dB) versus round-trip delay time (Fig. S1).

3.3. Dielectric Properties: Real Dielectric Constant

The round-trip travel time through a layer of known depth can be used to estimate the real dielectric constant ($\acute{\varepsilon}$) of the material. The DAF does not have many areas with substantial topographic relief, so there are few locations where depth can be measured at cross-sectional exposures. There are, however, a few collapse features in the DAF, specifically Sisyphi Cavi and Cavi Angusti (Ghatan and Head, 2004). These cavi, or eroded DAF materials, have several collapse levels that can be hypothesized to represent the same horizons as the adjacent reflectors, allowing calculation of a depth-averaged real dielectric constant ($\acute{\varepsilon}$) using the equation:

$$\acute{\varepsilon} = \left(\frac{c\Delta t}{2h}\right)^2 \qquad (1)$$

where h is the thickness of an exposure and Δt is the two-way time delay. Mars Orbiter Laser Altimeter (MOLA) Precision Experiment Data Record (PEDR) data are used to measure the thickness of the cavi collapse levels. Because Sisyphi Cavi and Cavi Angusti have multiple levels of collapse features, we obtain a range of real dielectric constant values.

4. Results

4.1. SHARAD

For the SHARAD dataset, 168 detections of subsurface reflectors were identified that coincided with the mapped extent of the DAF (Table S1). Most of the identified reflectors are limited in their length along a SHARAD ground track, but reflectors are identified across a wide range of longitudes (Fig. 1b). Higher concentrations of SHARAD reflectors are associated with generally lower two-way travel times (i.e. thinner materials). Because of the difference in vertical resolution and penetration depth between the instruments, it is not expected that the SHARAD and MARSIS reflectors necessarily correspond to the same subsurface interfaces. SHARAD detects at least one shallow interface in the DAF.

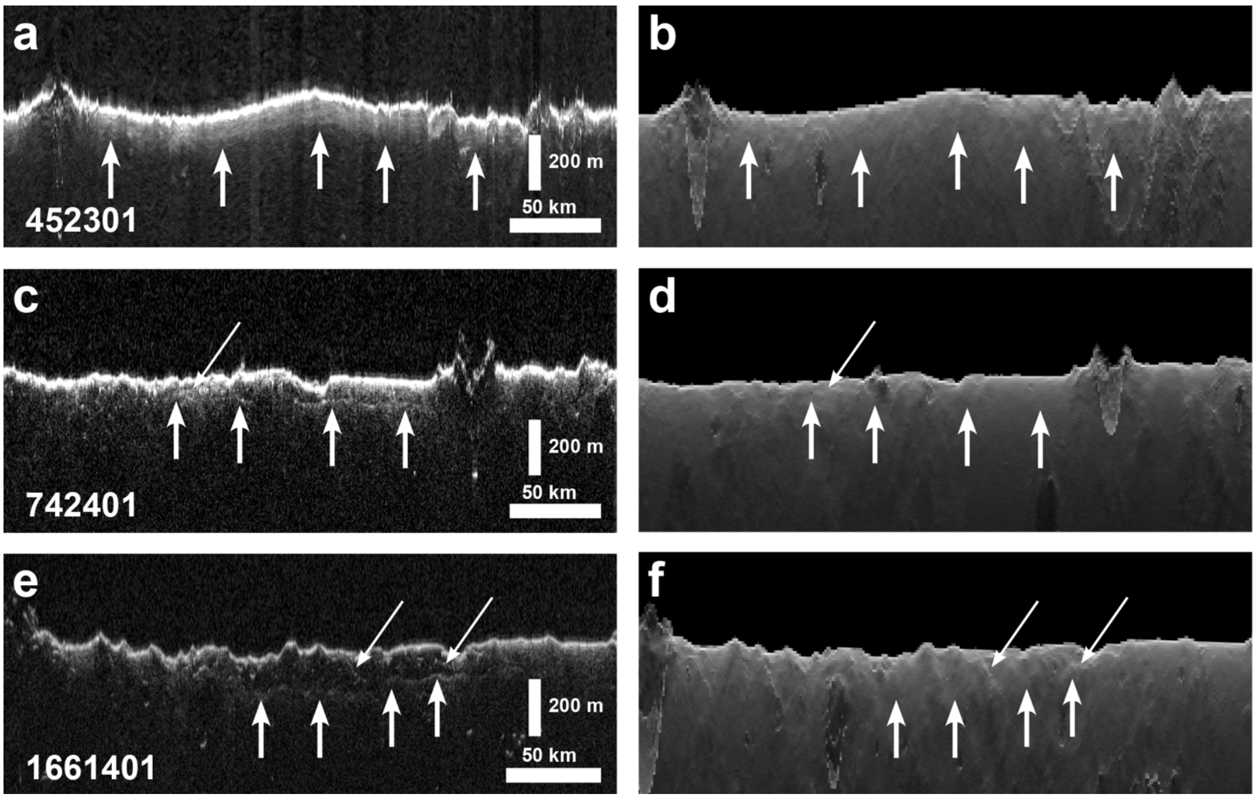

Figure 2. SHARAD reflectors and associated clutter simulations. (a, b) Shallow scattering zone, (c, d) a distinct subsurface reflector, and (e, f) a deeper distinct subsurface reflector. SHARAD radargrams are depth corrected assuming ε'=3.2 (e.g. Putzig et al., 2009). Radargram in (a) is a summed radargram (Whitten and Campbell, 2018), for improved signal to noise. Vertical white arrows indicate where reflectors are present in panels a, c, and e. Slanted thin white arrows (panels c–f) denote clutter, where an associated reflection is noted in the clutter simulations. These arrows are placed in the same location on the clutter simulations for comparison.

The characteristics of SHARAD subsurface reflections can be separated into two general categories: shallow scattering zones and distinct subsurface reflectors (Fig. 2). Each of these behaviors is identified across the DAF, though the shallow scattering zones are concentrated in Parva Planum (Fig. 1b). The shallow scattering behavior is defined by higher power values in the first ~1.3 μs to 1.9 μs after the surface echo (where 1.6 μs corresponds to a thickness of 85 m to 120 m for real dielectric constant values of ε'=4–8). While the shallow diffuse echoes might come from volume scattering or surface roughness, a few SHARAD tracks reveal fine-scale layering in these regions (Fig. 2a). Their overall appearance may thus be due to the overlap of echoes from interfaces separated by less than the vertical resolution (e.g. Lalich and Holt, 2017).

The distinct subsurface reflectors are approximately surface-parallel, well-focused, and each varies little in their depth along the ground track (Fig. 2c, e). In all cases mapped here, there is no evidence of off-nadir returns that can explain echoes inferred to arise in the subsurface (Fig. 2d, f). In several locations throughout the DAF, the material immediately below the SHARAD surface reflections appears dark in radargrams (Fig. 2e). This is due to generally weaker sidelobes that do not create the same radar bright values in the near-subsurface that is seen in radargrams with shallower reflectors (Fig. 2c). Many of these deeper distinct reflectors are lower in power and relatively diffuse, while others have a sharp transition from a radar-dark region to a brighter region (i.e. a region of more scattering).

Of the 168 SHARAD occurrences of subsurface reflectors, only 22 were obviously dipping over their length. Grouping several adjacent reflector detections, loss tangent calculations produce an average value of 0.005±0.003 for the DAF (Table S2). Loss tangent values for the distinct reflectors range from 0.002 to 0.009, with the deeper reflectors being associated with lower values in this range (Fig. 2e) and shallower distinct subsurface reflectors (Fig. 2c) generally on the higher end of this loss tangent range.

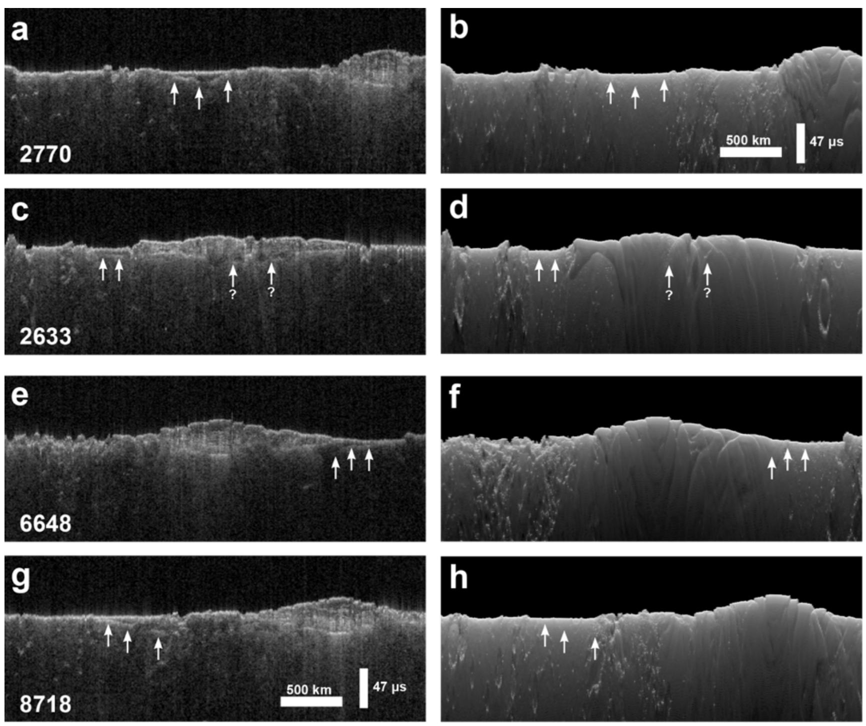

Figure 3. MARSIS reflectors that overlap with the DAF and associated clutter simulations. White arrows point to DAF reflectors. (a, b) Reflector has a general U-shape, starting at the surface and dipping into the subsurface before re-intersecting with the ground surface. (c, d) DAF reflector exterior to and below the SPLD (those below noted by '?'). (e, f) Reflector dipping underneath the SPLD in the Prometheus basin (right side). (g, h) Reflector dipping underneath Cavi Angusti. MARSIS radargrams are not depth corrected. Scale bars apply to all panels.

4.2. MARSIS

From 209 MARSIS tracks, 264 independent occurrences of subsurface reflectors were mapped and measured (Table S3). These MARSIS reflectors are found throughout the DAF, with the exception of areas north of 70°S around 0°E (Fig. 1b). In these regions, the lateral extent of the DAF is more constrained and interrupted by other geologic units (e.g. Cavi Angusti and Sisyphi Cavi). Mapped reflectors varied from near-surface-parallel interfaces to those that are U-shaped or dipping into the subsurface (Fig. 3). Additionally, the reflectors are well-focused, with no diffuse appearance. There is some evidence that MARSIS DAF reflectors continue underneath the SPLD, especially in the Prometheus basin (Fig. 3c, right side). Most MARSIS reflectors provide no evidence of subsurface layering in the DAF; material between the surface and subsurface reflectors appears homogeneous, having no obvious variations in appearance (e.g. intermediate reflectors or volume scattering).

The average DAF loss tangent value derived from all MARSIS data is 0.009±0.006 (Fig. 4, Table S4), but across the deposit values vary significantly (Fig. 4). The loss tangent was calculated for only those reflectors assigned a confidence level other than "none" (Text S2). Approximately 72% of the reliable DAF MARSIS reflectors yield loss tangent values >0.005, with lower values of 0.001–0.005 generally clustered in areas to the northwest of Cavi Angusti and southwest of Sisyphi Cavi (75.0°S, 272.0°E and 75.5°S, 340.0°E).

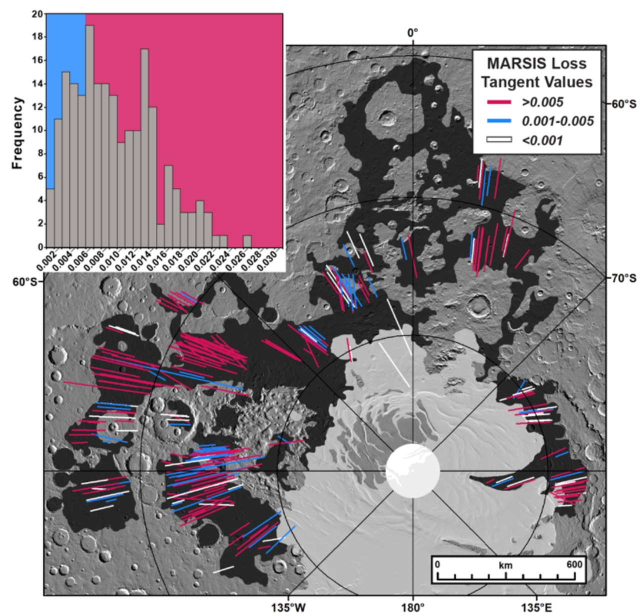

Figure 4. Distribution of MARSIS-derived loss tangent values across the DAF. Tracks with a loss tangent value >0.005 are shown in pink and those with values between 0.001 and 0.005 are in blue. Inset histogram shows the distribution of loss tangent values ≥0.001 for tracks with "high" and "moderate" confidences (Table S4). White lines show the location of reflectors with loss tangent values <0.001 (Table S4). Geologic units from Tanaka and Scott (1987) and Skinner et al. (2006). MOLA 128 ppd hillshade.

4.3. Real Dielectric Constant

Real dielectric constant values derived for the DAF using terrace-defined layer thicknesses from Cavi Angusti and Sisyphi Cavi with both MARSIS and SHARAD reflectors (Fig. S2) have a large range (Table S5). Some derived values are implausible for the assumed materials present in a three component system, namely pore space, water ice, and rock, which have dielectric constant values of 1, 3.15, and ~8, respectively, (Johari, 1976; Moore and Jakosky, 1989; Picardi et al., 2004; see Bramson et al., 2015 for an explanation of this method) (Table S5).

Four collapse terraces were identified both at Sisyphi Cavi and a cavi southeast of Pityusa Patera that could plausibly correspond to the depth of adjacent reflectors (Table S5; Fig. S2). The depths of each terrace differ somewhat between these two cavi regions. Considering both locations, the most plausible dielectric constant values are derived from "terrace 2" that has depths of 315 m and 274 m for Sisyphi and the Pityusa cavi, respectively (Table S5) and corresponding $\acute{\varepsilon}$ of 2.90±0.9 and 3.84±0.59 from SHARAD data. In general, MARSIS data did not yield realistic values, likely due to their coarse vertical spatial resolution.

5. Discussion and Conclusions

The DAF has variable surface roughness and is heterogeneous in subsurface properties, as evidenced by the two different radar echo behaviors observed in the SHARAD data (Fig. 2). Just north of Schmidt crater, around 66°S and 277°E, there is a dense cluster of tracks that exhibit deeper discrete subsurface reflectors (Fig. 2e). Several other SHARAD tracks have this behavior, but the density of tracks is much lower across the rest of the DAF. Additionally, clusters of SHARAD tracks with shallower, distinct, subsurface reflectors (Fig. 2c) are concentrated around South crater (77°S, 22°E), along the western edge of Parva Planum. The shallow scattering behavior is observed across the DAF but is also focused in Parva Planum, along the eastern edge of the deposit. Analysis of THEMIS IR daytime imagery does not indicate any obvious morphologic differences between the materials corresponding to these two categories of SHARAD reflectors.

While no obvious differences in near-surface scattering are noted in MARSIS data, some of the MARSIS reflectors mapped as DAF appear to dip below the south polar layered deposits (SPLD) in the Prometheus basin and also near Cavi Angusti (Fig. 3c). Subsurface reflectors extending underneath the SPLD represent a minority of the tracks analyzed, and the majority of these reflectors are within the Prometheus basin. Most other reflectors are located around the SPLD periphery and do not extend laterally very far beneath the SPLD. It is expected that the materials contained within Prometheus basin, and thus the DAF, would continue underneath the SPLD given that the cap covers the southernmost portion of the basin. Additionally, in the MARSIS data there are a few short segments of reflectors below the base of more central areas of SPLD (Fig. 3b, arrows with question marks) (Plaut et al., 2007b). While these data do not show sub-SPLD reflectors directly connected with MARSIS reflectors external to the SPLD they do suggest that the DAF is likely continuous beneath the SPLD.

The reported loss tangent values provide a significant additional constraint on the properties of the DAF. SHARAD data suggest an average loss tangent value of 0.005±0.003 for the DAF. MARSIS values can be broken into two groups: (1) 28% of values spanning 0.001–0.005 and (2) 72% of reflector-bounded materials exceeding a loss tangent of 0.005 (Fig. 4). The mean for all MARSIS observations is 0.009±0.006. The average value from MARSIS suggests that relatively volatile-poor material is predominant by comparison to the loss tangent range of 0.002–0.005

estimated by Plaut et al. (2007b) for icy deposits, and values of ~0.01 for sediments in Amazonis Planitia (Campbell et al., 2008; Campbell and Morgan, 2018) (Fig. 5).

Loss tangent determinations for other deposits on Mars show that the MFF, mid-latitude remnant glaciers (lobate debris aprons (LDA) and lineated valley fill (LVF)), and NPLD (Watters et al., 2007; Campbell et al., 2008; Grima et al., 2009; Campbell and Morgan, 2018) are all of lower loss than the DAF estimate from MARSIS (Fig. 5). Materials in Arcadia and Utopia Planitiae have intermediate loss values consistent with the MARSIS DAF results. The subsurface reflector-bounded materials in Arcadia and Utopia Planitiae have been interpreted to denote either the base of a massive ice-rich unit (Bramson et al., 2015; Stuurman et al., 2016) or a dominantly volatile-free material with a possible modest fraction of water ice (Campbell and Morgan, 2018). The DAF loss tangent from SHARAD leaves open the possibility of a greater amount of ice, but again not likely the dominant component. For example, a buried deposit of massive ice would lead to a plateau in estimated loss values (i.e., near the SHARAD estimates) beyond the onset of the nearly lossless material; instead, MARSIS data show depth-integrated values continue to rise with deeper probing. The DAF materials are thus interpreted to be predominantly volatile-poor, although some fraction of either distributed ice or discrete icy layers within the deposit are possible.

The thickness of the DAF varies substantially across the deposits, with maximum and minimum average reflector depths of 1600 m and 40 m, respectively. The reflectors within the DAF are some of the deepest detected with MARSIS, with an average depth of ~470 m (median average depth = 436 m), assuming an ε' of 5; an ε' of 5 was chosen based on the relatively low ice content of the DAF derived from average loss tangent values. Other deep reflectors in MARSIS or SHARAD data are generally associated with low-attenuation materials like water ice (Plaut et al., 2007b; Selvans et al., 2010) and the enigmatic Medusae Fossae Formation (MFF) (Watters et al., 2007; Campbell and Morgan, 2018). However, MARSIS signal penetration of 400–500 m is also observed in ice-free deposits like the basaltic sand in Meridani Planum (Watters et al., 2017). Thus, there is some ambiguity in distinguishing between the effects of porosity, compaction with depth, and water ice content on the depth-averaged loss tangent or real dielectric constant.

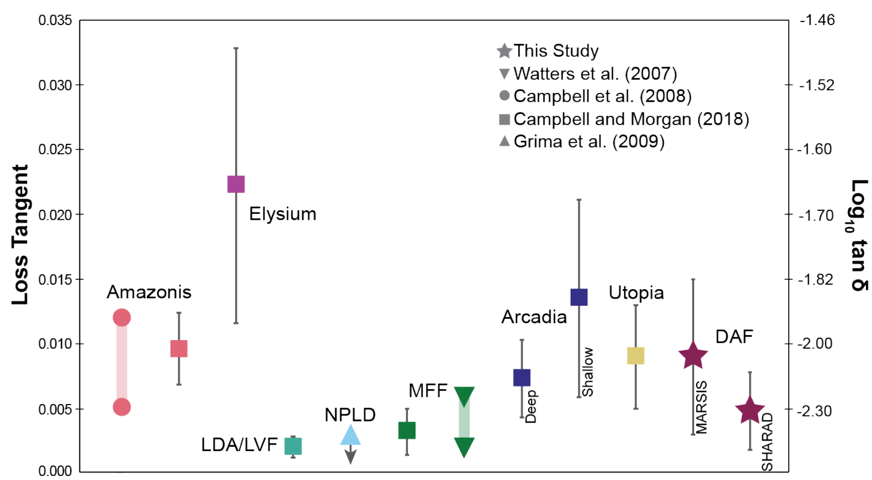

Figure 5. Comparison of the average loss tangent determined for the DAF and other units on Mars, including units interpreted as water ice-rich (NPLD, LDA/LVF), or sedimentary and

volcanic (e.g. Amazonis and Elysium Planitiae) (colored symbols denote different locations). Error bars are noted by thin black lines and thicker colored lines represent a range of loss tangent values reported in source publication. After Figure 3 in Campbell and Morgan (2018).

There is overwhelming evidence for past volatile-rich materials in the DAF. Assuming the DAF represents the dry remnants of a polar ice sheet that contained ~10% lithic material, similar to the SPLD (Plaut et al., 2007b; Zuber et al., 2007), an ancient DAF ice sheet had an approximate volume of ~7×10^6 km^3 (Text S3) and thickness of <5 km assuming the current DAF areal extent. The loss tangent results for the DAF suggest that a large portion of any such ice has been lost over its ~3.5 Ga existence and may not be preserved below the surface. If the subsurface is cold enough for long enough, ancient ice could be preserved (Bryson et al., 2008), but laboratory studies and observations of other massive ice deposits on Mars (e.g. Toon et al., 1980; Bramson et al., 2017) indicate that while lag deposits retard sublimation rates, it is still possible to lose large volumes of ice through this process over geologic time (Chevrier et al., 2007; Bryson et al., 2008), especially with increased insolation due to obliquity excursions (Levrard et al., 2004). Given the range of possible obliquity variations over the last 250 Myr (Laskar et al., 2004), the south polar region has experienced periods of increased insolation that would have led to the destabilization of subsurface ice, especially given that the average obliquity over this interval is ~34°. The loss tangent results presented here, combined with the morphology of superposed landforms and water ice distributions from Hesperian climate models (Wordsworth et al., 2013; Scanlon et al., 2018), indicate that there were volatiles in the near-surface (pedestal craters) and deep-subsurface (cavi) of the DAF in the past. However, over the lifetime of the DAF, a large fraction of its volatiles may have been lost due to climate variations caused by changes in the obliquity of Mars.

6. Acknowledgements

We thank the I.B. Smith and one anonymous reviewer for their constructive reviews of this work. This work was funded under JPL contracts to the MRO-SHARAD science team. The SHARAD instrument was provided to NASA's Mars Reconnaissance Orbiter (MRO) mission by the Italian Space Agency (ASI), and its operations are led by the DIET Department, University of Rome "La Sapienza" under an ASI contract. This work was funded under JPL contracts to the MRO-SHARAD science team. The authors thank the MRO mission team and the SHARAD instrument team for their efforts in acquiring the radar sounder data set. All data are publicly available. SHARAD radargrams can be found on the NASA Planetary Data System and MARSIS data are available on the ESA Planetary Science Archive.

7. References

Bleacher, J.E., Sakimoto, S.E., Garvin, J.B., Wong, M. (2003) Deflation/erosion rates for the Parva Member, Dorsa Argentea Formation and implications for the south polar region of Mars, *J. Geophys. Res.* 108, doi:10.1029/2001JE001535.

Boynton, W.V., Feldman, W.C., Squyres, S.W., Prettyman, T.H., Brückner, J., Evans, L.G., Reedy, R.C., Starr, R., Arnold, J.R., Drake, D.M., Englert, P.A.J., Metzger, A.E., Mitrofanov, I., Trombka, J.I., d'Uston, C., Wänke, H., Gasnault, O., Hamara, D.K., Janes, D.M., Marcialis, R.L., Maurice, S., Mikheeva, I., Taylor, G.J., Tokar, R., Shinohara (2002) Distribution of hydrogen in the near surface of Mars: Evidence for subsurface ice deposits, *Science* 297, 81–85. doi:10.1126/science.1073722.

Bramson, A.M. Byrne, S., Putzig, N.E., Sutton, S., Plaut, J.J., Brothers, T.C., Holt, J.W., (2015) Widespread excess ice in Arcadia Planitia, Mars, *Geophys. Res. Lett.* 42, 6566–6574. doi:10.1002/2015GL064844.

Bramson, A.M., Byrne, S., Bapst, J. (2017) Preservation of midlatitude ice sheets on Mars, *J. Geophysical Research, Planets* 122, 2250–2266. doi:10.1002/2017JE005357.

Bryson, K.L., Chevrier, V., Sears, D.W.G., Ulrich, R. (2008) Stability of ice on Mars and the water vapor diurnal cycle: Experimental study of the sublimation of ice through a fine-grained basaltic regolith, *Icarus* 196, 446–458. doi:10.1016/j.icarus.2008.02.011.

Butcher, F.E.G., Conway, S.J., Arnold, N.S., (2016) Are the Dorsa Argentea on Mars eskers? *Icarus* 275, 65–84. doi:10.1016/j.icarus.2016.03.028.

Campbell, B.A., Morgan, G.A. (2018) Fine-scale layering of Mars polar layered deposits and signatures of ice content in nonpolar material from multiband SHARAD data processing, *Geophys. Res. Lett.* 45, 1759–1766. doi:10.1002/2017GL075844.

Campbell, B.A., Watters, T.R. (2016) Phase compensation of MARSIS subsurface sounding data and estimation of ionospheric properties: New insights from SHARAD results, *J. Geophys. Res.* 121, 180–193, doi:10.1002/2015JE004917.

Campbell, B.A., Carter, L., Phillips, R., Plaut, J., Putzig, N., Safaeinili, A., Seu, R., Biccari, D., Egan, A., Orosei, R. (2008) SHARAD radar sound of the Vastitas Borealis, Formation in Amazonis Planitia, *J. Geophys. Res.* 113, E12010, doi:10.1029/2008JE003177.

Carter, L.M., Campbell, B.A., Holt, J.W., Phillips, R.J., Putzig, N.E., Mattei, S., Seu, R., Okubo, C.H., Egan, A.F. (2009) Dielectric properties of lava flows west of Ascraeus Mons, Mars, *Geophys. Res. Lett.* 36, L23204, doi:10.1029/2009GL041234.

Chevrier, V., Sears, D.W.G., Chittenden, J.D., Roe, L.A., Ulrich, R., Bryson, K., Billingsley, L., Hanley, J. (2007) Sublimation rate of ice under simulated Mars conditions and the effect of layers of mock regolith JSC Mars-1, *Geophys. Res. Lett.* 34, L02203. doi:10.1029/2006GL028401.

Choudhary, P., Holt, J.W., Kempf, S.D., (2016) Surface clutter and echo location analysis for the interpretation of SHARAD data from Mars, *IEEE* 13, 1285–1289. doi:10.1109/LGRS.2016.2581799.

Dickson, J., Head, J.W., (2006) Evidence for an Hesperian-aged South circum-polar lake margin environment on Mars, *Planet. Space Sci.* 54, 251–272, doi:10.1016/j.pss.2005.12.010.

Ghatan, G.J., Head, J.W. (2002) Candidate subglacial volcanoes in the south polar region of Mars: Morphology, morphometry, and eruption conditions, *J. Geophys. Res.* 107, E7,5048, doi:10.1029/2001JE001519.

Ghatan, G.J., Head, J.W. (2004) Regional drainage of meltwater beneath a Hesperian-aged south circumpolar ice sheet on Mars, *J. Geophys. Res.* 109, E07006, doi:10.1029/2003JE002196.

Grima, C., Kofman, W., Mouginot, J., Phillips, R.J., Hérique, A., Biccari, D., et al. (2009) North polar deposits of Mars: Extreme purity of the water ice, *Geophys. Res. Lett.* 36, L03203, doi:10.1029/2008GL036326.

Head, J.W., Pratt, S. (2001) Extensive Hesperian-aged south polar ice sheet on Mars: Evidence for massive melting and retreat, and lateral flow and ponding of meltwater, *J. Geophys. Res.* 106, 12275–12299, doi:10.1029/2000JE001359.

Howard, A.D., (1981) Etched plains and braided ridges of the south polar region of Mars: features produced by basal melting of ground ice, *Reports of the Planetary Geo. Program*, 286–288.

Johari, G.P. (1976). The dielectric properties of H_2O and D_2O ice Ih at MHz frequencies, *The Journal of Chemical Physics* 64, 3998–4005, doi:10.1063/1.432033.

Jöns, H.-P. (1992) Fossil glaciations in the environs of the south polar, Mars? Lunar Planet. Sci. Conf., 23rd, abstract 1314.

Kadish, S.J., Head, J.W., (2011) Preservation of layered paleodeposits in high-latitude pedestal craters on Mars, *Icarus* 213, 443–450. doi:10.1016/j.icarus.2011.03.029.

Kargel, J.S., Strom, R.G. (1992) Ancient glaciation on Mars, *Geology* 20, 3–7, doi:10.1130/0091-7613(1992)020<0003:AGOM>2.3.CO;2.

Kress, A.M., Head, J.W., (2015) Late Noachian and early Hesperian ridge systems in the south circumpolar Dorsa Argentea Formation, Mars: Evidence for two stages of melting of an extensive late Noachian ice sheet, *Planet. Space Sci.* 109, doi:10.1016/j.pss.2014.11.025.

Lalich, D.E., Holt, J.W. (2017) New martian climate constraints from radar reflectivity within the north polar layered deposits, *Geophys. Res. Lett.* 44, 657–664. doi:10.1002/2016GL071323.

Laskar, J., Correia, A.C.M., Gastineau, M., Joutel, F., Levrard, B., Robutel, P. (2004) Long term evolution and chaotic diffusion of the insolation quantities of Mars, *Icarus* 170, 343–364. doi:10.1016/j.icarus.2004.04.005.

Levrard, B., Forget, F., Montmessin, F., Laskar, J. (2004) Recent ice-rich deposits formed at high latitudes on Mars by sublimation of unstable equatorial ice during low obliquity, *Nature* 431, 1071–1075. doi:10.1038/nature03055.

Milkovich, S.M., Head, J.W., Pratt, S. (2002) Meltback of Hesperian-aged ice-rich deposits near the south pole of Mars: Evidence for drainage channels and lakes, *J. Geophys. Res.* 107, E65043, doi:10.1029/2001FE001JE001802.

Moore, H.J., Jakosky, B.M., (1989) Viking landing sites, remote-sensing observations, and physical properties of martian surface materials, *Icarus* 81, 164–184. doi:10.1016/0019-1035(89)90132-2.

Picardi, G., Biccari, D., Seu, R., Marinangeli, L., Johnson, W.T.K., Jordan, R.L., Plaut, J., Safaeinili, A. Gurnett, D.A., Ori, G.G., Orosei, R., Calabrese, D., Zampolini, E. (2004) Performance and surface scattering models for the Mars Advanced Radar for Subsurface and Ionosphere Sounding (MARSIS), *Planet. Space Sci.* 52, 149–156, doi:10.1016/j.pss.2003.08.020.

Plaut, J.J., Kahn, R., Guinnss, E.A., Arvidson R.E., (1988) Accumulation of sedimentary debris in the south polar region of Mars, and implications for climate history, *Icarus* 76, 357–377, doi: 10.1016/0019-1035(88)90076-0.

Plaut, J.J., Ivanov, A., Safaeinili, A., Milkovich, S.M., Picardi, G., Seu, R., Phillips, R. (2007a) Radar sounding of the subsurface layers in the south polar plains of Mars: Correlation with the Dorsa Argentea Formation, Lunar Planet. Sci. Conf., 38th, abstract 2144.

Plaut, J.J., Picardi, G., Safaeinili, A., Ivanov, A., Milkovich, S.M., Cicchetti, A., Kofman, W., Mouginot, J., Farrell, W.M., Phillips, R.J., Clifford, S.M., Frigeri, A., Orosei, R., Federico, C., Williams, I.P., Gurnett, D.A., Nielsen, E., Hagfors, T., Heggy, E., Stofan, E.R., Plettemeier, D., Watters, T.R., Leuschen, C.J., Edenhofer, P. (2007b) Subsurface radar sounding of the south polar layered deposits of Mars, *Science* 316, 92–95. doi:10.1126/science.1139672.

Putzig, N.E., Phillips, R.J., Campbell, B.A., Holt, J.W., Plaut, J.J., Carter, L.M., Egan, A.F., Bernardini, F., Safaeinili, A., Seu, R. (2009) Subsurface structure of Planum Boreum from Mars Reconnaissance Orbiter Shallow Radar soundings, *Icarus* 204, 443–457. doi: 10.1016/j.icarus.2009.07.034.

Scanlon, K.E., Head, J.W., Fastook, J.L., Wordsworth, R.D. (2018) The Dorsa Argentea Formation and the Noachian-Hesperian climate transition, *Icarus* 299, 339–363, doi:10.1016/j.icarus.2017.07.031.

Selvans, M.M., Plaut, J.J., Aharonson, O., Safaeinili, A. (2010) Internal structure of Planum Boreum, from Mars advanced radar for subsurface and ionospheric sounding data, *J. Geophys. Res.* 115, E09003. doi:10.1029/2009JE003537.

Seu, R., Biccari, D., Orosei, R., Lorenzoni, L.V., Phillips, R.J., Marinangeli, L., Picardi, G., Masdea, A., Zampolini, E., (2004), SHARAD: The MRO 2005 shallow radar, *Planet. Space Sci.* 52, 157–166. doi:10.1016/j.pss.2003.08.024.

Skinner, J.A., Jr, Hare, T.M., Tanaka, K.L. (2006) Digital renovation of the atlas of Mars 1:15,000,000-scale global geologic series maps, *Lunar Planet. Sci. Conf.* 37th, abstract 2331.

Tanaka, K.L., Scott, D.H. (1987) Geologic map of the polar regions of Mars, USGS IMAP 1802-C, 1:15M.

Tanaka, K.L., Kolb, E.J. (2001) Geologic history of the polar regions of Mars based on Mars Global Surveyor Data, *Icarus* 154, 3–21, doi:10.1006/icar.2001.6675.

Tanaka, K.L., Skinner, J.A., Jr., Dohm, J.M., Irwin, R.P., III, Kolb, E.J., Fortezzo, C.M., Platz, T., Michael, G.G., and Hare, T.M. (2014) Geologic map of Mars, USGS Scientific Investigations Map 3292, scale 1:20M, doi:10.3133/sim3292.

Toon, O.B., Pollack, J.B., Ward, W., Burns, J.A., Bilski, K. (1980), The astronomical theory of climate changes on Mars, *Icarus* 44, 552–607.

Watters, T.R., Campbell, B., Carter, L., Leuschen, C.J., Plaut, J.J., Picardi, G., Orosei, R., Safaeinili, A., Clifford, S.M., Farrell, W.M., Ivanov, A.B., Phillips, R.J., Stofan, E.R. (2007) Radar sounding of the Medusae Fossae Formation Mars: Equatorial ice or dry, low-density deposits?, *Science* 318, 1125–1128. doi:10.1126/science.1148112.

Watters, T.R., Leuschen, C.J., Campbell, B.A., Morgan, G.A., Cicchetti, A., Grant, J.A., Phillips, R.J., Plaut, J.J. (2017) Radar sounder evidence of thick, porous sediments in Meridiani Planum and implications for ice-filled deposits on Mars, *Geophys. Res. Lett.* 44, 9208–9215, doi:10.1002/2017GL074431.

Whitten, J.L., Campbell, B.A. (2018) Lateral continuity of layering in the Mars south polar layered deposits from SHARAD sounding data, *J. Geophys. Res. Planets* 123, 1541–1554. doi:10.1029/2018je005578.

Wordsworth, R., Forget, F., Millour, E., Head, J.W., Madeleine, J.-B., Charnay, B. (2013) Global modelling of the early martian climate under a denser CO_2 atmosphere: Water cycle and ice evolution, *Icarus* 222, 1–19. doi:10.1016/j.icarus.2012.09.036.

Zuber, M. T., Phillips, R. J., Andrews-Hanna, J. C., Asmar, S. W., Konopliv, A. S., Lemoine, F. G., et al. (2007) Density of Mars' South Polar Layered Deposits, *Science* 317, 1718–1719. doi:10.1126/science.1146995.